Catalysis Science & Technology

Accepted Manuscript

ROYAL SOCIETY
OF CHEMISTRY

www.rsc.org/catalysis

Submitted to *Catalysis Science & Technology* as an article **(revised)**

Molybdenum-doped α-MnO_2 as an efficient reusable heterogeneous catalyst for aerobic sulfide oxygenation

Tsubasa Uematsu, Yumi Miyamoto, Yoshiyuki Ogasawara, Kosuke Suzuki, Kazuya Yamaguchi and Noritaka Mizuno*

Department of Applied Chemistry, School of Engineering, The University of Tokyo,
7-3-1 Hongo, Bunkyo-ku, Tokyo 113-8656, Japan. E-mail: tmizuno@mail.ecc.u-tokyo.ac.jp

Abstract

Oxygenation of sulfides to sulfoxides and/or sulfones is an important transformation, and the development of efficient heterogeneous catalysts for the oxygenation, which can utilize O_2 as the terminal oxidant, is highly desired. In this study, we have successfully developed manganese oxide-based efficient heterogeneous catalysts for aerobic oxygenation of sulfides. Firstly, we prepared four kinds of manganese oxides possessing different crystal structures, such as α-MnO_2, β-MnO_2, γ-MnO_2, and δ-MnO_2, and their structure-activity relationships were examined for the aerobic oxygenation of thioanisole. Amongst them, α-MnO_2 showed the best catalytic performance for the oxygenation. Moreover, α-MnO_2 was highly stable during the catalytic oxygenation possibly due to the tunnel K^+ ions. In order to further improve the catalytic performance of α-MnO_2, substitutional doping of transition metal cations, such as Mo^{6+}, V^{5+}, Cr^{3+}, and Cu^{2+}, into the framework was carried out. Undoped α-MnO_2 possessed a fibrous morphology. When doping of high-valent transition metal cations, especially Mo^{6+}, the lengths of fibers drastically shortened to form grain-like aggregates of ultrafine nanocrystals, resulting in increasing the specific surface areas and the numbers of surface catalytically active sites. In the presence of Mo^{6+}-doped α-MnO_2 (Mo-MnO_2), various kinds of sulfides could efficiently be oxidized to the corresponding sulfoxides as the major products. The observed catalysis was truly heterogeneous, and Mo-MnO_2 could repeatedly be reused with keeping its high catalytic performance. Besides sulfide oxygenation, Mo-MnO_2 could efficiently catalyze several aerobic oxidative functional group transformations through single-electron transfer oxidation processes, namely, oxygenation of alkylarenes, oxidative α-cyanation of trialkylamines, and oxidative S-cyanation of benzenethiols.

Introduction

The development of highly efficient catalytic systems for oxygenation of sulfides has attracted much attention because the corresponding oxygenation products, both sulfoxides and sulfones, have widely been utilized as oxygen-transfer reagents, ligands in asymmetric catalysis, and important synthetic intermediates for natural products, biologically important molecules, and functional materials.[1] In addition, oxidative desulfurization has emerged as a promising method for removal of sulfur compounds from fuels and industrial effluents.[1g,1h] Generally, oxygenation of sulfides has been performed using metal oxide-, peracid-, or oxoacid-based stoichiometric oxidants. Instead of using such stoichiometric oxidants, the choice of greener oxidants, such as H_2O_2 and O_2, in combination with suitable catalysts has recently become the mainstream for oxygenation of sulfides.

Up to the present, a number of efficient transition metal catalysts have been developed for H_2O_2-based oxygenation of sulfides.[2] Importantly, the use of ubiquitous and the greenest O_2 is more desirable from the standpoint of green chemistry. Although several catalytic systems for aerobic oxygenation of sulfides have been reported to date,[3] they have several disadvantages in some cases; for example, (i) sacrificial reductants, e.g., aldehydes, are required, (ii) photo-irradiation is required, and/or (iii) most of them are homogeneous systems, and recovery and reuse of catalysts are very difficult.[3] As far as we know, there are only a few reports on heterogeneously catalyzed oxygenation of sulfides using O_2 as the terminal oxidant without any additives and photoirradiation; polyoxometalates,[4a] MoS_2/Ta_3N_5,[4b] and Au/MnO_{2-x}[4c] are the examples of the reported heterogeneous catalysts. However, they have quite a bit of room for improvement of their catalytic activities, selectivities, substrate scopes, and in particular reusabilities. Therefore, the development of reliable heterogeneous catalysts is still an important and challenging research subject.

Manganese oxides, including mixed oxides, have attracted tremendous research interests because of their potential use as electrode materials, magnetic materials, adsorbents, oxidants, catalysts, electrocatalysts, and catalyst supports.[5] In laboratory scale organic synthesis, manganese oxides have traditionally been utilized as stoichiometric oxidants. In recent years, the use of manganese oxides as heterogeneous catalysts for aerobic oxidation reactions has been receiving a lot of attention, and several efficient systems have been developed to date.[6] For example, α-MnO_2, including a manganese oxide octahedral molecular sieve (OMS-2), has typically utilized for oxidative dehydrogenation and single-electron transfer oxidation processes, such as oxidative dehydrogenation of alcohols and its related transformations,[6c–6e] oxygenation of alkylarenes,[6f] oxidative α-cyanation of tertiary amines,[6g] and oxidative homocoupling of thiols and its related transformations.[6h,6i] We have recently developed aerobic oxidative amidation of primary alcohols using aqueous NH_3 as the nitrogen source.[6j–6l] For the oxidative amidation, α-MnO_2 (OMS-2) showed the high catalytic performance, while β-MnO_2, γ-MnO_2, and δ-MnO_2 were not effective. For the oxidation of formaldehyde, the structure-activity relationships were carefully examined using α-MnO_2, β-MnO_2, γ-MnO_2, and δ-MnO_2, and amongst them, δ-MnO_2 was found to be the most active catalyst.[6m] In these manners, dramatic differences in catalytic performances among manganese oxides with different crystal structures have been observed with considerable frequency. Thus, the choice of kinds of manganese oxides for the target reaction is very crucial. In addition, the redox stability is also a very important factor for the catalytic use and repeated reuse of manganese oxides.

In this study, we prepared four kinds of manganese oxides with α-, β-, γ-, and δ-phase structures, and their structure-activity relationships were examined for the aerobic oxygenation of thioanisole. The difference in the catalytic performance was clearly observed among them, and α-MnO_2 showed the best catalytic performance and was highly stable during the oxygenation under aerobic and even anaerobic conditions. Furthermore, the performance of α-MnO_2 could be much improved by the substitutional doping of Mo^{6+} into the octahedral framework. In the presence of Mo^{6+}-doped α-MnO_2 (Mo-MnO_2), various kinds of structurally diverse sulfides including aromatic and aliphatic ones could efficiently be oxidized to the corresponding sulfoxides as the major products. The observed catalysis was truly heterogeneous, and Mo-MnO_2 could be reused for the oxygenation of thioanisole at least four times without an appreciable loss of its high catalytic performance. The structure of Mo-MnO_2 was intrinsically preserved after the repeated reuse for the oxygenation. Besides sulfide oxygenation, Mo-MnO_2 could act as an efficient heterogeneous catalyst for several aerobic oxidative functional group transformations through single-electron transfer oxidation processes, such as oxygenation of alkylarenes, oxidative α-cyanation of trialkylamines, and oxidative S-cyanation of benezenethiols.

Results and discussion

Structure-activity relationships for thioanisole oxygenation

To begin with, we prepared four kinds of manganese oxides with α-, β-, γ-, and δ-phase structures according to the previously reported procedures with minor modifications (see the Experimental section).[6k,6m,7] Their X-ray powder diffraction (XRD) patterns are shown in Fig. 1. The XRD pattern of α-MnO_2 could be well indexed to a cryptomelane-type manganese oxide with a 2 × 2 tunnel (4.6 Å × 4.6 Å) (JCPDS 29-1020). The XRD patterns of β-MnO_2 and γ-MnO_2 were in good agreement with those of pyrolusite-type (JCPDS 24-0735) and nsutite-type (JCPDS 14-0644) manganese oxides, respectively. The XRD pattern of δ-MnO_2 was characteristic of a birnessite-type manganese oxide with a layered structure (JCPDS 43-1456). Therefore, four types of manganese oxides with different crystal structures were successfully prepared. The peak widths and intensities of these XRD patterns imply that α-MnO_2 and β-MnO_2 possess relatively high crystallinities in comparison with γ-MnO_2 and δ-MnO_2. The specific surface areas of α-MnO_2, β-MnO_2, γ-MnO_2, and δ-MnO_2 were 80 $m^2\ g^{-1}$, 18 $m^2\ g^{-1}$, 73 $m^2\ g^{-1}$, and 124 $m^2\ g^{-1}$, respectively (Table 1). The manganese contents in α-MnO_2 (52.5 wt%) and δ-MnO_2 (47.4 wt%) were somewhat lower than those in β-MnO_2 (64.3 wt%) and γ-MnO_2 (62.0 wt%) (Table 1), which is mainly due to the accommodation of K^+ ions into the 2 × 2 tunnel of α-MnO_2 or into the interlayer of δ-MnO_2.[8] The average oxidation state (AOS, determined by redox titration) of α-MnO_2 was 3.77 and slightly lower than those of the others

(3.90–3.92) (Table 1), suggesting the compensation of the mixed valency of manganese by the tunnel K^+ ions (or H^+).[8]

By using these manganese oxide catalysts, their structure-activity relationships were examined for the oxygenation of thioanisole (**1a**). The reactions were performed in *o*-dichlorobenzene at 150 ºC (bath temperature) under aerobic (O_2: 5 atm) or anaerobic (Ar: 1 atm) conditions. The results are summarized in Table 2. Under aerobic conditions, the oxygenation selectively proceeded to afford methyl phenyl sulfoxide (**2a**) with trace amounts of methyl phenyl sulfone (**3a**) in all cases, and the order of the catalytic performances from the viewpoint of the product yields was as follows; α-MnO_2 (41%) ≈ γ-MnO_2 (42%) > δ-MnO_2 (29%) > β-MnO_2 (12%) (the values in the parentheses are the total yields of **2a** and **3a**; Table 2, entries 1, 3, 5, and 7). The yields did not simply increase with increasing in their specific surface areas. The low catalytic performance of β-MnO_2 is probably owing to its low specific surface area. Under anaerobic conditions, the oxygenation hardly proceeded when using α-MnO_2 and δ-MnO_2 (Table 2, entries 2 and 8), indicating that O_2 is effectively utilized as the terminal oxidant in these cases. In other words, the electron-transfer from the reduced manganese species to O_2 can smoothly proceed in the case of α-MnO_2 and δ-MnO_2. In the case of γ-MnO_2, **2a** was produced in a significant amount (11%) even under anaerobic conditions (Table 2, entry 6), thus suggesting that γ-MnO_2 can effectively utilize its lattice oxygen species for the oxygenation of **1a** in addition to the use of O_2.

The XRD patterns of these manganese oxides retrieved after the oxygenation of **1a** under the conditions described in Table 2 were measured in order to confirm their redox stabilities. With regard to α-MnO_2, the peak positions, widths, and intensities were almost unchanged after the use for the oxygenation under both aerobic and anaerobic conditions, as shown in Fig. 2. Thus, the crystal structure and crystallinity of α-MnO_2 were specifically preserved after the oxygenation. Moreover, α-MnO_2 could be reused for the oxygenation of **1a** without an appreciable loss of its catalytic performance (Table 2, entry 9). Although the peak positions were almost unchanged after the use of δ-MnO_2 for the oxygenation, the peak intensities much decreased, suggesting that the crystallinity of δ-MnO_2 was lowered after the oxygenation (Fig. S1). In contrast, the different phases and the significant peak shifts were observed after the oxygenation in the case of β-MnO_2 and γ-MnO_2 (Fig. S1). In particular, γ-MnO_2 was partly converted into a redox inactive manganite phase (MnO(OH), JCPDS 41-1379) after the use under anaerobic conditions (Fig. S1). Even when γ-MnO_2 was utilized for the aerobic oxygenation, the XRD peaks significantly shifted toward lower angle (Fig. S1), suggesting the lattice enlargement due to the reduction of manganese species. In addition, we confirmed that the AOS of γ-MnO_2 much decreased from 3.90 to 3.42 even after the use for the aerobic oxygenation (Table S1). These analyses imply that the redox stabilities for the oxygenation of **1a** decrease in the order of α-MnO_2 > δ-MnO_2 > β-MnO_2 > γ-MnO_2. Manganese oxides possessing the accommodated K^+ ions, such as α-MnO_2 and δ-MnO_2, showed relatively high redox stabilities. The temperature-programmed reduction (TPR) measurements using H_2 were performed for these manganese oxide samples. The peaks in these TPR profiles correspond to the sequential reduction of MnO_2, that is, $MnO_2 \rightarrow Mn_2O_3 \rightarrow Mn_3O_4 \rightarrow MnO$. The TPR measurements revealed that the reduction temperature increased in the order of γ-MnO_2 < β-MnO_2 < δ-MnO_2 < α-MnO_2 (Fig. S2). This result showed that the reducibility sequence is γ-MnO_2 > β-MnO_2 > δ-MnO_2 > α-MnO_2, which is closely correlated with the redox stabilities.

As above-mentioned, γ-MnO_2 can act as an effective "oxidant" likely because its lattice oxygen species can effectively be utilized for the oxygenation of **1a** (Table 2, entry 6). The result of TPR analysis of γ-MnO_2 also supports the idea (Fig. S2). From the data of the oxygenations under aerobic and anaerobic conditions (Table 2, entries 5 and 6), the AOSs of γ-MnO_2 before and after the oxygenation (Table S1), and the elemental analysis (Table 1), we estimated that the production of **2a** via the "stoichiometric" oxygenation using the lattice oxygen species was 12 % and the production of **2a** via the "catalytic" oxygenation using O_2 was 29 % in the case of γ-MnO_2. However, once the active lattice oxygen species were consumed for the oxygenation, their regeneration (reoxidation) using O_2 was quite difficult under the present conditions, resulting in the formation of the reduced redox inactive phases, e.g., manganite phase. In addition, when reusing γ-MnO_2, a significant decrease in the performance was observed; the yield of **2a** dropped to 25% (Table 2, entry 11). Therefore, the catalytic use and repeated recycling of γ-MnO_2 for the oxygenation are difficult. We consider that the redox stability of manganese oxides is one of the most important factors for the catalytic use for this type of oxygenations and that the accommodated K^+ ions would play an important role on the stabilization of the manganese oxide framework structures. Indeed, in the case of stable α-MnO_2, the yield of **2a** for the reuse experiment was almost the same as that of the first run with as-prepared fresh α-MnO_2 (Table 2, entries 1 and 9). As above-mentioned, α-MnO_2 gave **2a** mostly through the catalytic oxygenation using O_2. Consequently, α-MnO_2 was the best catalyst for the oxygenation of **1a** among manganese oxides examined from the viewpoints of both the product yield (catalytic activity) and the redox stability. In order to further improve the performance of α-MnO_2, substitutional doping of additional transition metal cations into the framework was next carried out.

Substitutional doping into the framework of α-MnO_2

Substitutional doping of additional metal cations into the metal oxide framework is one of the most commonly utilized strategies to improve their catalytic properties. To date, substitutional doping of various transition metal cations into the framework of α-MnO_2 (including OMS-2) has been studied.[9] Doping of metal cations into α-MnO_2 possibly occurs in the octahedral framework and/or in the tunnel, which is largely dependent on the crystal radii (CR) and the coordination geometries of dopant cations. Six-coordinated cations with the similar sizes as those of Mn^{4+} (the Shannon–Prewitt CR[10]: 0.67 Å) and Mn^{3+} (0.72 Å for low spin species, 0.785 Å for high spin species) can readily be introduced into the octahedral framework, while relatively larger cations tend to be introduced into the tunnel.[11a,11b,11e,11g] In this study, we attempted to introduce several transition metal cations with different CRs and valences, that is, Mo^{6+}, V^{5+}, Cr^{3+}, and Cu^{2+}. According to the previous reports, the following substitution patterns can be expected.[9j,11] With regard to six-coordinated high-valent dopant cations, such as Mo^{6+} (0.73 Å) and V^{5+} (0.68 Å), the framework substitution may occur, which likely causes the formation of manganese vacancies.[9j,11c,11d] On the other hand, when doping of six-coordinated low-valent cations, such as Cr^{3+} (0.755 Å) and Cu^{2+} (0.87 Å), is performed, the net negative charge of the α-MnO_2 octahedral framework increases, and thereby protonation of oxygen atoms to form surface OH species and/or increasing the amounts of the tunnel cations would occur for the charge compensation.[9j,11a] There is some possibility of introducing relatively larger Cu^{2+} (0.87 Å) into the tunnel of α-MnO_2.[11f,11g]

Four kinds of metal-doped α-MnO_2 catalysts (given in the format: M-MnO_2) were prepared essentially by the same procedure for α-MnO_2; 5 mol% (with respect to total metals) precursor solutions of K_2MoO_4, $NaVO_3$, $Cr(CH_3COO)_3 \cdot H_2O$, and $CuSO_4 \cdot 5H_2O$ were utilized for the preparation of Mo-MnO_2, V-MnO_2, Cr-MnO_2, and Cu-MnO_2, respectively (see the Experimental section). As shown in Fig. 3, the XRD patterns of M-MnO_2 were specifically the same as that of α-MnO_2, and no additional peaks attributed to segregated phases of MoO_3, V_2O_5, Cr_2O_3, and CuO were observed. The XRD peak intensities of Mo-MnO_2 were slightly weaker than those of the others (Fig. 3), suggesting the low crystallinity and/or the formation of smaller crystals of Mo-MnO_2. Fig. 4 shows the Raman scattering spectra of α-MnO_2 and M-MnO_2. All the observed Raman bands could be attributed to the Mn–O lattice vibrations within the MnO_6 octahedral double chains in α-MnO_2, and the strong bands typically observed for segregated phases of MoO_3 (around 820 cm^{-1}), V_2O_5 (around 990 cm^{-1}), Cr_2O_3 (around 550 cm^{-1}), and CuO (around 290 cm^{-1}) were not detected.[12] The Raman band around 390 cm^{-1} was assignable to the Mn–O bending vibrations.[8a] The intense two bands around 575 cm^{-1} and 635 cm^{-1} were attributed to the symmetric Mn–O vibrations, thus indicating the formation of a well-developed tetragonal structure with an interstitial space consisting of 2 × 2 tunnels in these M-MnO_2 samples.[8a] It has been reported that the Raman band around 635 cm^{-1} is related to the Mn–O vibrations perpendicular to the direction of the MnO_6 octahedral double chains and that the band is significantly damped by the presence of heavy tunnel cations.[8a] As shown in Fig. 4, the relative intensities of the bands around 575 cm^{-1} and 635 cm^{-1} for M-MnO_2 were almost the same as those for α-MnO_2, indicating that these dopant cations are introduced not into the tunnels but mostly into the octahedral frameworks. From these XRD and Raman analyses, we consider that all four M-MnO_2 samples possess pure cryptomelane-type phases with dopant cations in their octahedral frameworks. The contents of the dopant cations in Mo-MnO_2 and V-MnO_2 were 5.0 mol% and 5.2 mol% (Table 3), respectively, and the same as those of the precursor solutions (5 mol%). In contrast, the contents of the dopant cations in Cr-MnO_2 and Cu-MnO_2 were 2.0 mol% and 2.5 mol%, respectively (Table 3), and smaller than those of the precursor solutions (5 mol%). This is likely because of the difference in the substitution patterns of dopant cations, as above-mentioned. The contents of potassium in these M-MnO_2 were 3.52–4.14 wt% (Table 3).

The specific surface areas of Mo-MnO_2, V-MnO_2, Cr-MnO_2, and Cu-MnO_2 were 212 $m^2\ g^{-1}$, 120 $m^2\ g^{-1}$, 91 $m^2\ g^{-1}$, and 109 $m^2\ g^{-1}$, respectively (Table 3), and larger than that of undoped α-MnO_2 (80 m^2 g^{-1}). The significantly large surface area of Mo-MnO_2 (212 m^2 g^{-1}) is likely attributed to its small crystalline size (Fig. 5b). The XPS spectra in the Mn 2p region showed no significant difference among α-MnO_2 and M-MnO_2 (Fig. S3). This indicated that the AOSs on these surface were almost the same. The XPS spectra in the O 1s region are shown in Fig. S4. Each O 1s spectrum can be deconvoluted into three peaks corresponding to the three types of surface oxygen species; the low (around 530 eV), medium (around 531 eV), and high binding energy peaks (around 532 eV) are ascribed to the coordinatively saturated lattice oxygen species (described as O_{sat}), the coordinatively unsaturated oxygen species (e.g., OH and adsorbed oxygen species on the surface, described as O_{unsat}), and adsorbed molecular H_2O on the surface, respectively.[6d] The curve-fitting analyses of these XPS spectra showed that the $O_{unsat}/(O_{sat} + O_{unsat})$ values for α-MnO_2, Mo-MnO_2, V-MnO_2, Cr-MnO_2, and Cu-MnO_2 were 0.24, 0.18, 0.25, 0.26, and 0.31, respectively (Table S2). In addition, the content of potassium in Cu-MnO_2 was significantly lower than those in the others (Table 3). Thus, the surface concentration of coordinatively unsaturated oxygen species (possibly OH species) in Cu-MnO_2 was somewhat larger than those in the others.

The transmission electron microscopy (TEM) images indicated that undoped α-MnO_2 possessed a fibrous morphology (Fig. 5a). The average length and width of the fibers were 500 ± 100 nm and 20 ± 5 nm, respectively, and the lattice fringe spacing of 4.9 Å attributed to the (200) plane was observed throughout the α-MnO_2 sample. The similar fibrous morphologies were also observed when doping of low-valent metal cations, such as Cr^{3+} and Cu^{2+}, and in these cases the lattice fringe spacings of 6.9 Å due to the (110) planes were clearly observed (Fig. 5d,e). The average lengths of the fibers in Cr-MnO_2 and Cu-MnO_2 were almost the same as that in α-MnO_2, while these widths (15 ± 5 nm) were somewhat thinner than that in α-MnO_2 (20 ± 5 nm). As shown in Fig. 5b,c, when doping of high-valent metal cations, such as Mo^{6+} and V^{5+}, the lengths of fibers drastically shortened, especially in the case of Mo-MnO_2, resulting in the formation of grain-like aggregates of ultrafine nanocrystals. Their larger specific surface areas (Table 3) are possibly caused by the formation of the aggregates of nanocrystals. Such morphologies were also observed in Mo-MnO_2 and V-MnO_2 samples possessing lower dopant contents (2.5 mol%) (Fig. S5). The TEM image of Mo-MnO_2 displayed clear lattice fringes throughout the sample. Fortunately, we could successfully observe the *c*-axis view (2 × 2 tunnel view) of Mo-MnO_2, which was well consistent with the simulated structure (Fig. 5b).

Catalytic performance and scope of metal-doped α-MnO_2

The catalytic activities of Mo-MnO_2, V-MnO_2, Cr-MnO_2, and Cu-MnO_2 were compared for the aerobic oxygenation of **1a** under the conditions described in Table 4. Among the M-MnO_2 catalysts examined, Mo-MnO_2 showed the highest catalytic performance, and the performance was much superior to that of undoped α-MnO_2; the oxygenation of **1a** using Mo-MnO_2 gave the corresponding sulfoxide **2a** and sulfone **3a** in 75% and 3% yields, respectively (Table 4, entry 2), while undoped α-MnO_2 gave **2a** and **3a** in 40% and 1% yields, respectively (Table 4, entry 1). The total yield of **2a** and **3a** obtained with V-MnO_2 (46%) were slightly higher than that with α-MnO_2 (41%) (Table 4, entry 3). The substantial improvement of the catalytic activity of α-MnO_2 by doping of low-valent metal cations, such as Cr^{3+} and Cu^{2+}, was hardly observed (Table 4, entries 4 and 5), thus suggesting that increasing the surface concentration of OH species is not crucial for the oxygenation. Therefore, the substitutional doping of high-valent metal cations, especially Mo^{6+}, was an effective strategy for improvement of the catalytic performance of α-MnO_2 for this type of oxygenation reactions.

K_2MoO_4 (precursor for Mo-MnO_2) showed no activity for the oxygenation of **1a** (Table 5, entry 4). The catalytic activities of simple physical mixtures of K_2MoO_4 and α-MnO_2 (Table 5, entry 5) as well as MoO_3 and α-MnO_2 (Table 5, entry 6) were intrinsically the same as that of α-MnO_2 (Table 5, entry 1). Moreover, a supported catalyst, Mo^{6+}/α-MnO_2, prepared by impregnation of Mo^{6+} species onto α-MnO_2 was not effective for the oxygenation of **1a** (Table 5, entry 3). Thus, molybdenum compounds themselves are essentially inactive for the oxygenation. Again, we emphasize that the substitutinal doping of Mo^{6+} into the framework is crucial for improvement of the catalytic performance of α-MnO_2. As above-described, the α-MnO_2 structure showed the best performance among examined manganese oxides with various crystal structures. This is principally owing to the highly stabilized structure by the tunnel K^+ ions. We consider that the manganese vacancies formed by the doping of high-valent cations,[9j,11c,11d] especially Mo^{6+}, may prevent the growth of α-MnO_2 crystals along the *c*-axis direction. Although the *c*-axis growth was significantly suppressed, the local crystallinity was intrinsically preserved, as evidenced by the above-mentioned XRD, Raman, and TEM analyses. As a result, the grain-like aggregates of ultrafine nanocrystals of metal-doped α-MnO_2 were formed, and the specific surface areas increased in these cases. This kind of morphology possibly provides a large number of surface catalytically active sites in α-MnO_2, e.g., vacancy sites, effective for the oxygenation, that is, electron-transfers from a substrate to the catalyst and from the reduced catalyst to O_2.

By using the most effective Mo-MnO_2, the scope of aerobic oxygenation with respect to various kinds of structurally diverse sulfides was next investigated. The results are summarized in Table 6. Thioanisole (**1a**) and its derivatives, which possess electron-donating as well as electron-withdrawing substituents at each position of the benzene rings (**1b**–**1e**), could efficiently be converted into the corresponding sulfoxides in moderate to high yields as the major products with concomitant formation of the corresponding sulfones (Table 6, entries 1–5). Diphenyl sulfide (**1f**) afforded the corresponding sulfoxide in a high yield (Table 6, entry 6). It should be noted that not only aryl sulfides but also a less reactive alkyl one (**1g**) could efficiently be oxygenated (Table 6, entry 7). In order to verify whether the observed catalysis was derived from solid Mo-MnO_2 or leached metal species (manganese and/or molybdenum), Mo-MnO_2 was removed by filtration during the reaction at 3 h, and then the reaction was again carried out with the filtrate under the same reaction conditions. As shown in Fig. S6, the production of **2a** was completely stopped by the removal of Mo-MnO_2. In addition, we confirmed by the inductively coupled plasma atomic emission spectroscopy (ICP-AES) analysis that manganese and molybdenum species were not present in the filtrate (below 0.1%). These experimental evidences can rule out any contribution to the observed catalysis from metal species that leached into the reaction solution, and the observed catalysis for the present oxygenation is truly heterogeneous.[13] After the reaction of **1a** was completed, Mo-MnO$_2$ could readily be retrieved from the reaction mixture by simple filtration. The XRD analysis revealed that the crystal structure and crystallinity of Mo-MnO$_2$ were intrinsically preserved after the repeated reuse for the oxygenation of **1a** (Fig. 6). Furthermore, Mo-MnO$_2$ could be reused for the same reaction at least four times with keeping its high catalytic performance (Fig. 7).

The Mo-MnO$_2$-catalyzed oxygenation of **1a** was strongly suppressed by the presence of a radical scavenger of 2,6-di-*tert*-butyl-4-methylphenol (40 mol%) (9% yield of **2a** under the conditions described in Table 5), indicating that radical intermediates are possibly involved in the present sulfide oxygenation. It is known that manganese oxides can generate cation radical species from heteroatom-containing compounds, such as thiols and amines, through single-electron transfer (SET) oxidation. Similarly, in the present case, cation radical species are possibly generated by SET oxidation of sulfides. Then, the reduced Mo-MnO$_2$ is reoxidized by the SET to O$_2$, and a superoxide anion radical species is likely formed.[6f,6g] By the reaction of the sulfide cation radical and the superoxide anion radical species, the corresponding sulfoxides are successively obtained as the final products.[14]

Besides sulfide oxygenation, Mo-MnO$_2$ could efficiently catalyze several aerobic oxidative functional group transformations through SET oxidation processes. Benzylic oxygenation of alkylarenes, such as xanthene, fluorene, and diphenylmethane, efficiently proceeded to give the corresponding ketones in moderate to high yields (Fig. 8a). The oxygenation proceeds through SET oxidation/deprotonation, followed by oxygen insertion.[6f] Mo-MnO$_2$ could act as an efficient heterogeneous catalyst for oxidative α-cyanation of trialkylamines using trimethylsilyl cyanide (TMSCN) as the cyano source and O$_2$ as the terminal oxidant. The cyanation regioselectively took place at the α-methyl positions, giving the corresponding α-amino nitriles in high yields (Fig. 8b). The cyanation possibly proceeds through the following mechanism.[6g] Firstly, an amine cation radical is formed by SET. Then, deprotonation of the cation radical to form an α-aminated carbon radical. This step is stereoelectronically controlled and determines the above-mentioned regioselectivity to the α-methyl position.[6g] Then, the second SET proceeds to form an iminium cation, followed by nucleophilic trap by CN$^-$ species to afford the corresponding α-amino nitrile. Moreover, in the presence of Mo-MnO$_2$, thiocyanates could be synthesized in almost quantitative yields starting from benzenethiols under very mild conditions (Fig. 8c). The present cyanation proceeds through the Mo-MnO$_2$-catalyzed oxidative homocoupling of benzenethiols to the corresponding disulfides through SET oxidation, followed by nucleophilic bond cleavage to produce the desired thiocyanates and thiolate species.[6i] Mo-MnO$_2$ can catalyze oxidative homocoupling of the thiolate species, thus resulting in quantitative production of thiocyanates formally from benzenethiols.[6i]

Conclusion

In this work, we have obtained several important findings for the manganese oxide-based catalyst design and the application of manganese oxide catalysts to several aerobic oxidation reactions. Firstly, we prepared four kinds of manganese oxides possessing different crystal structures, namely α-MnO_2, β-MnO_2, γ-MnO_2, and δ-MnO_2, and examined their structure-activity relationships for the aerobic oxygenation of thioanisole. Amongst these manganese oxides, α-MnO_2 showed the best catalytic performance and was highly durable during the catalytic oxygenation possibly due to the stabilization of its framework structure by the tunnel K^+ ions. The performance of α-MnO_2 could be further improved by the substitutional doping of Mo^{6+} into the octahedral framework. By the doping of Mo^{6+}, manganese vacancies were likely formed, which would prevent the growth of α-MnO_2 crystals along the *c*-axis direction. Although the *c*-axis growth was suppressed, the local crystallinity was essentially preserved. Consequently, the grain-like aggregates of ultrafine nanocrystals were formed in the case of Mo^{6+}-doped α-MnO_2 (Mo-MnO_2), resulting in increasing the specific surface area. This kind of morphology would afford a large number of surface catalytically active sites, for example, vacancy sites, effective for the oxygenation. In the presence of Mo-MnO_2, various kinds of structurally diverse sulfides including aromatic and aliphatic ones could be oxidized to the corresponding sulfoxides as the major products using O_2 as the terminal oxidant. The observed catalysis of Mo-MnO_2 was shown to be a truly heterogeneous fashion, and Mo-MnO_2 could be reused for the oxygenation of thioanisole at least four times with keeping its high catalytic performance. The structure of Mo-MnO_2 was intrinsically preserved after the repeated reuse for the oxygenation. The present sulfide oxygenation was likely initiated by single-electron transfer (SET) oxidation process. Aside from sulfide oxygenation, Mo-MnO_2 could efficiently catalyze several aerobic oxidative functional group transformations through SET oxidation processes, such as oxygenation of alkylarenes, oxidative α-cyanation of trialkylarenes, and oxidative S-cyanation of benzenthiols.

Experimental section

Materials

$KMnO_4$, $NaVO_3$, concentrated HNO_3, and KOH were purchased from Kanto Chemical. $MnSO_4 \cdot H_2O$ was purchased from Aldrich. K_2MoO_4 and MoO_3 were purchased from Wako Pure Chemical Industries. $Cr(CH_3COO)_3 \cdot H_2O$ was purchased from Nacalai Tesque. $(NH_4)_2S_2O_8$ was purchased from Tokyo Chemical Industry. Substrates, solvents, and naphthalene (internal standard for GC analysis) were purchased from Tokyo Chemical Industry, Kanto Chemical, or Aldrich. All reagents were used as received without further purification. TBA_2MoO_4 (TBA = tetra-*n*-butylammonium) was prepared according to the reported procedure with modification.[15] Manganese oxide catalysts were prepared by the procedures described below.

Preparation of manganese oxide catalysts

α-MnO_2 was prepared according to the following procedure.[6k] An aqueous solution (100 mL) of $KMnO_4$ (5.89 g) was added to an aqueous solution (30 mL) of $MnSO_4 \cdot H_2O$ (8.8 g) and concentrated HNO_3 (3 mL). The resulting mixture was refluxed at 100 °C for 24 h. Then, the dark brown solid formed was filtered off, washed with a large amount of water, and dried under open air at 150 °C, affording 7.5 g of α-MnO_2. Metal-doped α-MnO_2 catalysts (M-MnO_2) were prepared intrinsically the same procedure for non-doped α-MnO_2. For the preparation of M-MnO_2, a dopant metal source (K_2MoO_4, $NaVO_3$, $Cr(CH_3COO)_3 \cdot H_2O$, or $CuSO_4 \cdot 5H_2O$) was initially added to the $MnSO_4 \cdot H_2O$ solution (2.5 or 5 mol% with respect to total metals), then followed by the above procedure, affording 7–8 g of M-MnO_2. In the case of α-MnO_2, the mixed valency of manganese can be compensated by K^+ (or H^+).

β-MnO_2 was prepared according to the following procedure.[6m] An aqueous solution (80 mL) containing $MnSO_4 \cdot H_2O$ (1.69 g) and $(NH_4)_2S_2O_8$ (2.28 g) was stirred at room temperature for 30 min. Then, the mixture was transferred to a Teflon vessel. The vessel was attached inside an autoclave, and the solution was heated at 140 °C for 12 h. The dark brown solid formed was filtered off, washed with a large amount of water, and dried under open air at 150 °C, affording 0.8 g of β-MnO_2.

γ-MnO_2 was prepared according to the following procedure.[6m] An aqueous solution (80 mL) containing $MnSO_4 \cdot H_2O$ (3.375 g) and $(NH_4)_2S_2O_8$ (4.575 g) was stirred at room temperature for 30 min. Then, the mixture was transferred to a Teflon vessel. The vessel was attached inside an autoclave, and the solution was heated at 90 °C for 24 h. The dark brown solid formed was filtered off, washed with a large amount of water, and dried under open air at 150 °C, affording 1.5 g of γ-MnO_2.

δ-MnO_2 was prepared according to the following procedure.[7] An aqueous solution (200 mL) containing ethanol (92 mL) and KOH (33.6 g) was added dropwise to an aqueous solution (150 mL) of $KMnO_4$ (9.48 g). The mixture was stirred at room temperature for 1 h, followed by heating at 80 °C for 48 h. The dark brown solid was formed was filtered off, washed with a large amount of water, and dried under open air at 80 °C, affording 9.0 g of δ-MnO_2. It is possible that K^+ and OH^- can be introduced into the interlayer of δ-MnO_2.

A supported catalyst, Mo^{6+}/α-MnO_2, was prepared by impregnation of Mo^{6+} species onto α-MnO_2. α-MnO_2 (1.0 g) was dispersed in an acetonitrile solution (30 mL) of TBA_2MoO_4 (0.337 g). After stirring for 30 min, acetonitrile was evaporated to dryness, affording 1.0 g of Mo^{6+}/α-MnO_2. The molybdenum content in Mo^{6+}/α-MnO_2 was 2.7 wt%.

Characterization of manganese oxide catalysts

The contents of manganese and dopant metals in manganese oxide samples were determined by ICP-AES analyses using a Shimadzu ICPS-8100 apparatus. The contents of potassium in manganese oxide samples were determined by atomic absorption spectrometry analyses using a Hitachi Z 2000 apparatus. The AOSs of manganese were determined by redox titration, during which manganese in the sample was reduced with excess $Fe(NH_4)_2(SO_4)_2$, and unreacted Fe^{2+} was titrated with an aqueous solution of $KMnO_4$. This redox titration was repeated three times for each sample, and the AOSs were defined as average values. BET surface areas were measured by N_2 adsorption at −196 °C using a micromeritics ASAP 2010 instrument. XRD patterns were recorded using a Rigaku SmartLab instrument under Cu Kα radiation (λ = 1.5418 Å, 45 kV, 200 mA). XPS analyses were performed using a JEOL JPS-9000 apparatus under Mg Kα radiation (*hν* = 1253.6 eV, 8 kV, 10 mA). The peak positions were calibrated by Au 4f 7/2 peak (84 eV) of deposited on the grid. The baselines were subtracted by the Shirley method. Raman spectra were measured on a Nippon Bunko NRS-5100 Raman apparatus using a 532 nm laser. TEM images were obtained using a JEM-2000EX II apparatus at an acceleration voltage of 200 kV. TEM specimens were prepared by dispersing manganese oxide samples in ethanol and sonicating them for 30 min before deposition on carbon-coated copper grid. TPR profiles were measured on a BELCAT apparatus with a quadrupole mass spectrometer. The sample was pretreated at 150 °C in a flow of Ar (30 mL min^{-1}) for 20 min. After the pretreatment, a mixed gas of H_2 and Ar (H_2: 7 vol%) was allowed to flow into the sample (30 mL min^{-1}) with progress of temperature from 100 to 550 °C at a rate of 10 °C min^{-1}. The amount of consumed H_2 was quantified by a mass spectrometer with the fragment of $m/z = 2$.

Catalytic reactions

GC quantitative analyses were performed on a Shimadzu GC-2014 apparatus with a FID detector equipped with a TC-1 or TC-5 capillary column. GC-MS analyses for product identification were performed on a GCMS-QP2010 apparatus at an ionization voltage of 70 eV equipped with a Inert-Cap 5 capillary column.

Oxygenation of sulfides was typically carried out as follows. Manganese oxide catalyst (25–50 mg), sulfide (0.5 mmol) *o*-dichlorobenzene (1 mL), and naphthalene (internal standard, 0.2 mmol) were placed in a Teflon vessel. The Teflon vessel was attached inside an autoclave, and the reaction was performed at 150 °C (bath temperature) in 5 atm of O_2 for 3–96 h. After the reaction was completed, the spent catalyst was separated by filtration and washed with acetone. Then, the filtrate was analyzed. The products were confirmed by comparison of their GC retention times and GC-MS spectra with those of authentic data. The spent catalyst was washed with acetone and water, and dried under open air at room temperature before being used for the reuse experiment. As for oxygenation of sulfides under anaerobic conditions and other oxidation reactions were carried out using a Schlenk-type reactor. These procedures were essentially the same as that for aerobic sulfide oxygenation.

Acknowledgements

We thank Mr. S. Torii (The University of Tokyo) for his help with preliminary experiments. This work was supported in part by Grants-in-Aid for Scientific Research from the Ministry of Education, Culture, Science, Sports, and Technology of Japan.

References and notes

1 (*a*) H. L. Holland, *Chem. Rev*., 1988, **88**, 357. (*b*) M. C. Carreño, *Chem. Rev*., 1995, **95**, 1717. (*c*) I. Fernández, N. Khiar, *Chem. Rev*., 2003, **103**, 3651. (*d*) R. F. D. L. Pradilla, I. Colomer, A. Viso, *Org. Lett*., 2012, **14**, 3068. (*e*) K. Hiroi, Y. Suzuki, I. Abe, R. Kawagishi, *Tetrahedron*, 2000, **56**, 4701. (*f*) S. Caron, W. Dugger, S. G. Ruggeri, J. A. Ragan, D. H. B. Ripin, *Chem. Rev*., 2006, **106**, 2943. (*g*) S. Otsuki, T. Nanoka, N. Takashima, W. Qian, A. Ishihara, T. Imai, T. Kabe, *Energy Fuels*, 2000, **14**, 1232. (*h*) Y. Shiraishi, H. Hara, T. Hirai, I. Komasawa, *Ind. Eng. Chem. Res*., 1999, **38**, 1589.

2 (*a*) D. Edwards, J. B. Stenlake, *J. Chem. Soc*., 1954, 3272. (*b*) F. G. Bordwell, P. J. Boutan, *J. Am. Chem. Soc*., 1957, **79**, 717. (*c*) M. Madesclaire, *Tetrahedron*, 1986, **42**, 5459. (*d*) Y. Watanabe, T. Numata, S. Oae, *Synthesis*, 1981, 204. (*e*) J. Drabowicz, M. Mikolafczyk, *Synthesis*, 1978, 758. (*f*) M. Jafarpour, M. Ghahramoninezhad, A. Rezaeifard, *RSC Adv*., 2014, **4**, 1601. (*g*) B. Machura, J. Palion, J. Mroziński, B. Kalińska, M. Amini, M. M. Najafpour, R. Kruszynski, *Polyhedron*, 2013, **53**, 132. (*h*) A. Rezaeifard, R. Haddad, M. Jafarpour, M. Hakimi, *ACS Sustainable Chem. Eng*., 2014, **2**, 942.

3 (*a*) T. Punniyamurthy, S. Velusamy, J. Iqbal, *Chem. Rev*., 2005, **105**, 2329. (*b*) I. V. Khavrutskii, G. M. Maksimov, O. A. Kholdeeva, *React. Kinet. Catal. Lett*., 1999, **66**, 325. (*c*) X. Zhou, H. Ji, *Catal. Commun*., 2014, **53**, 29. (*d*) H. Kawasaki, S. Kumer, G. Li, C. Zeng, D. R. Kauffman, J. Yoshimoto, Y. Iwasaki, R. Jin, *Chem. Mater*., 2014, **26**, 2777. (*e*) W. Li, L. Li, H. Xiao, R. Qi, Y. Huang, Z. Xie, X. Jing, H. Zhang, *RSC. Adv*., 2013. **3**, 13417. (*f*) W.-P. To, Y. Liu, T.-C. Lau, C.-M. Che, *Chem. –Eur. J*., 2013, **19**, 5654. (*g*) J. Dad′ová, E. Svobodová, M. Sikorski, B. König, R. Cibulka, *ChemCatChem*, 2012, **4**, 620. (*h*) H. Zhang, G. Wang, *Tetrahedron Lett*., 2014, **55**, 56. (*i*) S. E. Martín, L. I. Rossi, *Tetrahedron Lett*., 2001, **42**, 7147. (*j*) Y. Yuan, X. Shi, W. Liu, *Synlett*., 2011, **4**, 559. (*k*) H. Zhang, C. Chen, R. Liu, Q. Xu, W. Zhao, *Molecules*, 2010, **15**, 83. (*l*) N. Komatsu, M. Uda, H. Suzuki, *Chem. Lett*., 1997, 1229. (*m*) H. Zhang, C. Chen, R. Liu, *Synth. Commun*., 2012, **42**, 811. (*n*) A. M. Khenkin, G. Letius, R. Neurman, *J. Am. Chem. Soc*., 2010, **132**, 11446. (*o*) B. Li, A.-H. Liu, L.-N. He, Z.-Z. Yang, J. Gao, K.-H. Chen, *Green Chem*., 2012, **14**, 130. (*p*) I. Gamba, S. Palavicini, E. Monzani, L. Casella, *Chem. –Eur. J*., 2009, **15**, 12932. (*q*) H. B. Lee, T. Ren, *Inorg. Chim. Acta*, 2009, **362**, 1467. (*r*) M. Costas, C. W. Cady, S. V. Kryatov, M. J. Ryan, E. V. Rybak-Akimova, L. Que Jr., *Inorg. Chem*., 2003, **42**, 7519. (*s*) D. P. Riley, P. E. Correa, *J. Chem. Soc., Chem. Commun*., 1986, 1097. (*t*) K. Suzuki, J. Jeong, K. Yamaguchi, N. Mizuno, *New. J. Chem*., DOI: 10.1039/c5nj01045d.

4 (*a*) N. M. Okun, T. M. Anderson, C. L. Hill, *J. Am. Chem. Soc*., 2003, **125**, 3194. (*b*) Q. Gao, C. Giordano, M. Antonietti, *Angew. Chem*., *Int. Ed*., 2012, **51**, 11740. (*c*) A. Taketoshi, P. Concepción, H. García, A. Corma, M. Haruta, *Bull. Chem. Soc. Jpn*., 2013, **86**, 1412.

5 (*a*) F. Cheng, J. Chen, X. Gou, P. Shen, *Adv. Mater.*, 2005, **17**, 2753. (*b*) D. Zhan, Q. Zhang, X. Hu, T. Peng, *RSC Adv.*, 2013, **3**, 5141. (*c*) J. Ge, L. Zhuo, F. Yang, B. Tang, L. Wu, C. Tung, *J. Phys. Chem. B*, 2006, **110**, 17854. (*d*) L. Espinal, W. Wong-Ng, J. A. Kaduk, A. J. Allen, C. R. Snyder, C. Chiu, D. W. Siderius, L. Li, E. Cockayne, A. E. Espinal, S. L. Suib, *J. Am. Chem. Soc.*, 2012, **134**, 7944. (*e*) J. Yuan, X.Liu, O. Akbulut, J. Hu, S. L. Suib, J. Kong, F. Stellacci, *Nat. Nanotech.*, 2008, **3**, 332. (*f*) A. J. Fatiadi, *Synthesis*, 1976, 65. (*g*) J. R. Kona, C. K. King'ondu, A. R. Howell, S. L. Suib, *ChemCatChem*, 2014, **6**, 749. (*h*) D. M. Robinson, Y. B. Go, M. Mui, G. Gardner, Z. Zhang, D. Mastrogiovanni, E. Garfunkel, J. Li, M. Greenblatt, G. C. Dismukes, *J. Am. Chem. Soc.*, 2013, **135**, 3494. (*i*) F. Cheng, Y. Su, J. Liang, Z. Tao, J. Chen, *Chem. Mater.*, 2010, **22**, 898. (*j*) Q. Ye, J. Zhao, F. Huo, D. Wang, S. Cheng, T. Kang, H. Dai, *Microporous Mesoporous Mater.*, 2013, **172**, 20. (*k*) T. Takashima, K. Hashimoto, R. Nakamura, *J. Am. Chem. Soc.*, 2012, **134**, 18153. (*l*) A. Yamaguchi, R. Inuzuka, T. Takashima, T. Hayashi, K. Hashimoto, R. Nakamura, *Nat. Commun.*, 2014, **5**, 4256.

6 (*a*) L. Jin, C.-H. Chen, V. M. B. Crisostomo, L. Xu, Y.-C. Son, S. L. Suib, *Appl. Catal. A*, 2009, **355**, 169. (*b*) P. Pal, A. K. Giri, H. Singh, S. C. Ghosh, A. B. Panda, *Chem. Asian J.*, 2014, **9**, 2392. (*c*) Y.-C. Son, V. D. Makwana, A. R. Howell, S. L. Suib, *Angew. Chem.*, *Int. Ed.*, 2001, **40**, 4280. (*d*) J. Nie, H. Liu, *J. Catal.*, 2014, **316**, 57. (*e*) Z.-Z. Yang, J. Deng, T. Pan, Q.-X. Guo, Y. Fu, *Green Chem.*, 2012, **14**, 2986. (*f*) N. N. Opembe, Y.-C. Son, T. Sriskandakumar, S. L. Suib, *ChemSusChem*, 2008, **1**, 182. (*g*) K. Yamaguchi, Y. Wang, N. Mizuno, *ChemCatChem*, 2013, **5**, 2835. (*h*) S. Dharmarathna, C. K. King'ondu, L. Pahalagedara, C.-H. Kuo, Y. Zhang, S. L. Suib, *Appl. Catal. B Environ.*, 2014, **147**, 124. (*i*) K. Yamaguchi, K. Sakagami, Y. Miyamoto, X. Jin, N. Mizuno, *Org. Biomol. Chem.*, 2014, **12**, 9200. (*j*) K. Yamaguchi, H. Kobayashi, T. Oishi, N. Mizuno, *Angew. Chem.*, *Int. Ed.*, 2012, **51**, 544. (*k*) K. Yamaguchi, H. Kobayashi, Y. Wang, T. Oishi, Y. Ogasawara, N. Mizuno, *Catal. Sci. Technol.*, 2013, **3**, 318. (*l*) Y. Wang, H. Kobayashi, K. Yamaguchi, N. Mizuno, *Chem. Commun.*, 2012, **48**, 2642. (*m*) J. Zhang, Y. Li, L. Wang, C. Zhang, H. He, *Catal. Sci. Technol.*, 2015, **5**, 2305.

7 A. Iyer, J. Del-Pilar, C. K. King'ondu, E. Kissel, H. F. Garces, H. Huang, A. M. El-Sawy, P. K. Dutta, S. L. Suib, *J. Phys. Chem. C*, 2012, **116**, 6474.

8 (*a*) T. Gao, M. Glerup, F. Krumeich, R. Nesper, H. Fjellvåg, P. Norby, *J. Phys. Chem. C*, 2008, **112**, 13134. (*b*) J. E. Post, *Proc. Natl. Acad. Sci. USA*, 1999, **96**, 3447. (*c*) Y. Ma, J. Luo, S. L. Suib, *Chem. Mater.*, 1999, **11**, 1972. (*d*) A.-C. Gaillot, D. Flot, V. A. Drits, A. Manceau, M. Burghammer, B. Lanson, *Chem. Mater.*, 2003, **15**, 4666.

9 (*a*) A. M. A. Hashem, H. A. Mohamed, A. Bahloul, A. Eid, C. Julien, *Ionics*, 2008, **14**, 7. (*b*) R. Jothiramalingam, B. Viswanathan, T. K. Varadarajan, *J. Mol. Catal. A*, 2006, **252**, 49. (*c*) J. Cai, J. Liu, W.S. Willis, S. L. Suib, *Chem. Mater.*, 2001, **13**. 2413. (*d*) C. Calvert, R. Joesten, K. Ngala, J. Villegas, A. Morey, X. Shen, S. L. Suib, *Chem. Mater.*, 2008, **20**, 6382. (*e*) M. Polverejan, J. C. Villegas, S. L. Suib, *J. Am. Chem. Soc.*, 2004, **126**, 7774. (*f*) S. Ching, P. F. Driscoll, K. S. Kieltyka, M. R. Marvel, S. L. Suib, *Chem. Commun.*, 2001, 2486. (*g*) W. Y.

Hernández, M. A. Centeno, S. Ivanova, P. Eloy, E. M. Gaigneaux, J. A.Odriozoola, *Appl. Catal. B*, 2012, **123**, 27. (*h*) X. Tang, Y. Li, J. Chen, Y. Xu, W. Shen, *Microporous Mesoporous Mater.*, 2007, **103**, 250. (*i*) Z. Liu , Y. Xing, C.-H. Chen, L. Zhao, S. L. Suib, *Chem. Mater*., 2008, **20**, 2069. (*j*) C. K. King'ondu, N. Opembe, C.-H. Chen, K. Ngala, H. Huang, A. Iyer, H. F. Garcés, S. L. Suib, *Adv. Funct. Mater*., 2011, **21**, 312. (*k*) H. Zhou, Y. F. Shen, J. Y. Wang, X. Chen, C.-L. O'Young, S. L. Suib, *J. Catal.*, 1998, **189**, 321.

10 R. D. Shannon, *Acta Crystallogr.*, 1976 , **A32** , 751.

11 (*a*) L. R. Pahalagedara, S. Dharmarathna, C. K. King'ondu, M. N. Pahalagedara, Y.-T. Meng, C.-H. Kuo, S. L. Suib, *J. Phys. Chem. C*, 2014, **118**, 20363. (*b*) Q. Feng, H. Kanoh, Y. Miyai, K. Ooi, *Chem. Mater*., 1995, **7***,* 148. (*c*) M. Polverejan, J. C. Villegas, S. L. Suib, *J. Am. Chem. Soc*., 2004, **126**, 7774. (*d*) X. Tang, J. Li, J. Hao, *Catal. Commun*., 2010, **11**, 871. (*d*) X. Tang, J. Li, J. Hao, *Catal. Commun*., 2010, **11**, 871. (*e*) Y. Tanaka, M. Tsuji, *Solvent Extraction Ion Exchange*, 1997, **15**, 709. (*f*) X. Chen, Y.-F. Shen, S. L. Suib, C. L. O'Young, *Chem. Mater*., 2002, **14**, 940. (*g*) Y. Li, Z. Fan, J. Shi, Z. Liu, J. Zhou, W. Shangguan, *Catal. Today*, 2015, **256**, 178.

12 (*a*) L. Seguin , M. Figlarz , R. Cavagnat J.-C. Lassègues, *Spectrochim. Acta A*, 1995, **51**, 1323. (*b*) C. V. Ramana, R. J. Smith, O. M. Hussain, M. Massot, C. M. Julien, *Surf. Interface Anal*., 2005, **37**, 406. (*c*) M. Schraml-Marth, A. Wokaun, H. E. Curry-Hyde, A. Baiker, *J. Catal*., 1992, **133**, 415. (*d*) D. Chen, G. Shen, K. Tang, Y. Qian, *J. Cryst. Growth*, 2003, **254**, 225.

13 R. A. Sheldon, M. Wallau, I.W. C. E. Arends, U. Schuchardt, *Acc. Chem. Res*., 1998, **31**, 485.

14 (*a*) E. Baciocchi, T. D. Giac-co, F. Elisei, M. F. Gerini, M. Guerra, A. Lapi, P. Liberali, *J. Am. Chem. Soc*., 2003, **125**, 16444. (*b*) S. M. Bonsei, I. Manet, M. Freccero, M. Fagnoni, A. Albini, *Chem. –Eur. J*., 2006, **12**, 4844.

15 H. Sunaba, K. Kamata, N. Mizuno, *ChemCatChem*, 2014, **6**, 2333.

Table 1 Properties of manganese oxides

Entry	Catalyst	BET surface area (m^2 g^{-1})	Content (wt%)		AOS
			Mn	K	
1	α-MnO_2	80	52.5	4.07	3.77
2	β-MnO_2	18	64.3	–	3.90
3	γ-MnO_2	73	62.0	–	3.90
4	δ-MnO_2	124	47.4	7.78	3.92

Table 2 Oxygenation of **1a** using various manganese oxides

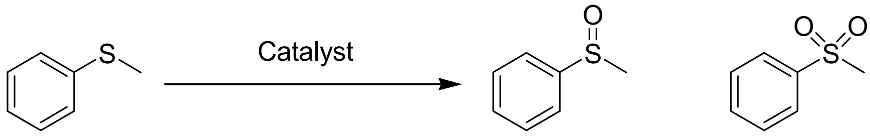

1a **2a** **3a**

Entry	Catalyst (mol%)[a]	Atmosphere [b]	Time (h)	Conv. of **1a** (%)	Yield (%)	
					2a	**3a**
1	α-MnO_2 (9.8)	O_2	24	45	40	1
2	α-MnO_2 (9.8)	Ar	96	4	4	<1
3	β-MnO_2 (2.3)	O_2	24	15	12	<1
4	β-MnO_2 (2.3)	Ar	96	6	1	<1
5	γ-MnO_2 (9.0)	O_2	24	43	41	1
6	γ-MnO_2 (9.0)	Ar	96	18	11	<1
7	δ-MnO_2 (14.1)	O_2	24	34	24	5
8	δ-MnO_2 (14.1)	Ar	96	9	<1	<1
9[c]	α-MnO_2	O_2	24	41	36	1
10[c]	β-MnO_2	O_2	24	17	13	<1
11[c]	γ-MnO_2	O_2	24	47	25	<1
12[c]	δ-MnO_2	O_2	24	36	30	2

Reaction conditions: Catalyst (25 mg), **1** (0.5 mmol), *o*-dichlorobenzene (1 mL), 150 °C (bath temp.). [a] The values in the parentheses are based on the surface exposed manganese species estimated from the specific surface areas and the crystal structures. [b] O_2 (5 atm) or Ar (1 atm). [c] Reuse experiments. These experiments used the retrieved catalyst. Conversions and yields were determined by GC analysis using naphthalene as an internal standard.

Table 3 Properties of M-MnO_2

Entry	Catalyst	BET surface area ($m^2\ g^{-1}$)	Content (wt%)		M/(Mn+M) (mol%)
			Mn	K	
1	α-MnO_2	80	52.5	4.07	–
2	Mo-MnO_2	212	51.1	3.60	5.0
3	V-MnO_2	120	55.3	4.15	5.2
4	Cr-MnO_2	91	57.6	4.04	2.0
5	Cu-MnO_2	109	56.9	3.53	2.5

Table 4 Oxygenation of **1a** using M-MnO_2

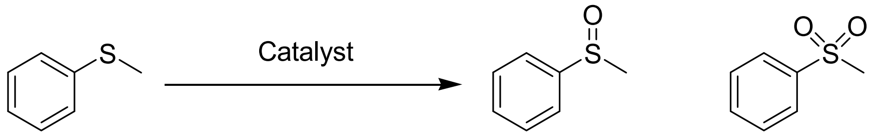

1a **2a** **3a**

Entry	Catalyst (mol%)[a]	Conv. of **1a** (%)	Yield (%)	
			2a	**3a**
1	α-MnO_2 (9.8)	45	40	1
2	Mo-MnO_2 (25.9)	82	75	3
3	V-MnO_2 (14.6)	46	45	1
4	Cr-MnO_2 (11.1)	47	40	1
5	Cu-MnO_2 (13.3)	40	38	1

Reaction conditions: Catalyst (25 mg), **1a** (0.5 mmol), *o*-dichlorobenzene (1 mL), 150 °C (bath temp.), O_2 (5 atm), 24 h. Conversions and yields were determined by GC analysis using naphthalene as an internal standard. [a] The values in the parentheses are based on the surface exposed manganese species estimated from the specific surface areas and the crystal structures.

Table 5 Oxygenation of **1a** using various catalysts

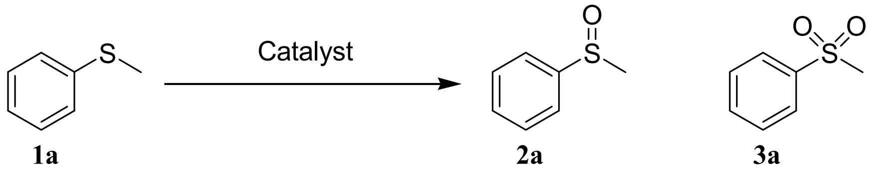

Entry	Catalyst	Mo/(Mn+Mo) (mol%)	Conv. of **1a** (%)	Yield (%)	
				2a	**3a**
1	α-MnO_2	–	27	24	1
2	Mo-MnO_2	5.0	40	37	1
3	Mo/α-MnO_2	4.7	9	3	<1
4	K_2MoO_4	–	6	<1	<1
5[a]	α-MnO_2 + K_2MoO_4	5.0	28	25	1
6[b]	α-MnO_2 + MoO_3	5.0	25	25	<1

Reaction conditions: Catalyst (25 mg), **1a** (0.5 mmol), *o*-dichlorobenzene (1 mL), O_2 (5 atm), 150 °C (bath temp.), 3 h. Conversions and yields were determined by GC analysis using naphthalene as an internal standard. [a] α-MnO_2 (25 mg) + K_2MoO_4 (2.8 mg). [b] α-MnO_2 (25 mg) + MoO_3 (1.8 mg).

Table 6 Scope of the Mo-MnO_2-catalyzed oxygenation of sulfides

Entry	Substrate		Product		Time (h)	Yield (%) [a]
1	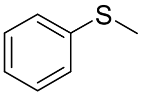	**1a**	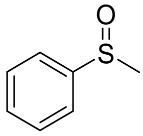	**2a**	6	73 (4)
2	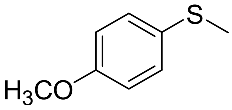	**1b**	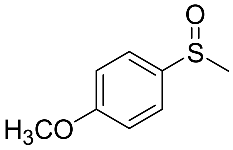	**2b**	6	91 (6)
3	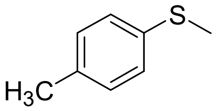	**1c**	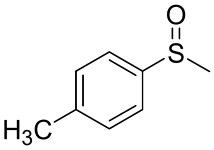	**2c**	24	76 (4)
4	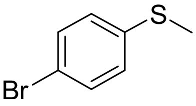	**1d**	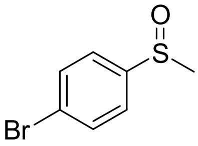	**2d**	24	77 (11)
5	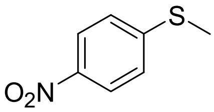	**1e**	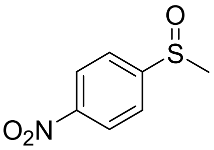	**2e**	24	40 (11)
6	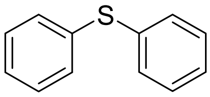	**1f**	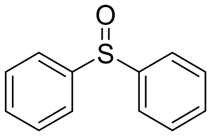	**2f**	24	90 (10)
7	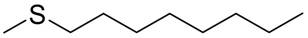	**1g**	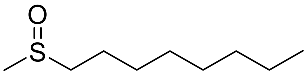	**2g**	24	53 (1)

Reaction conditions: Mo-MnO_2 (50 mg), **1** (0.5 mmol), *o*-dichlorobenzene (1 mL), 150 ºC (bath temp.), O_2 (5 atm). Yields were determined by GC analysis using naphthalene as an internal standard. [a] The values in the parentheses are the yields of the corresponding sulfones.

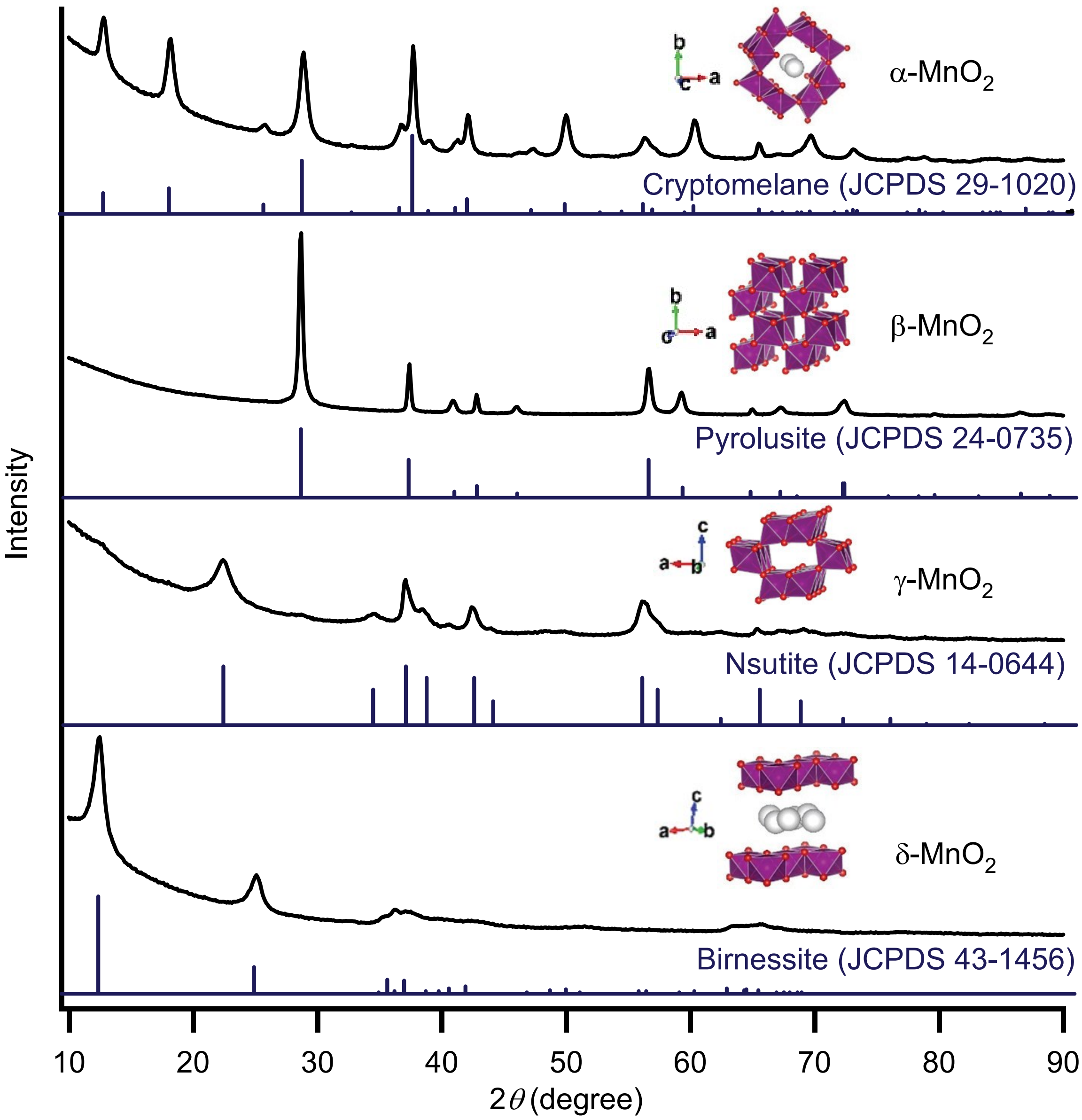

Fig. 1 XRD patterns and polyhedral representations of α-MnO_2, β-MnO_2, γ-MnO_2, and δ-MnO_2. Purple octahedra represent {$Mn^{3+}O_6$} or {$Mn^{4+}O_6$}. Red spheres represent oxygen atoms. White spheres represent accomodated K^+ ions or water molecules.

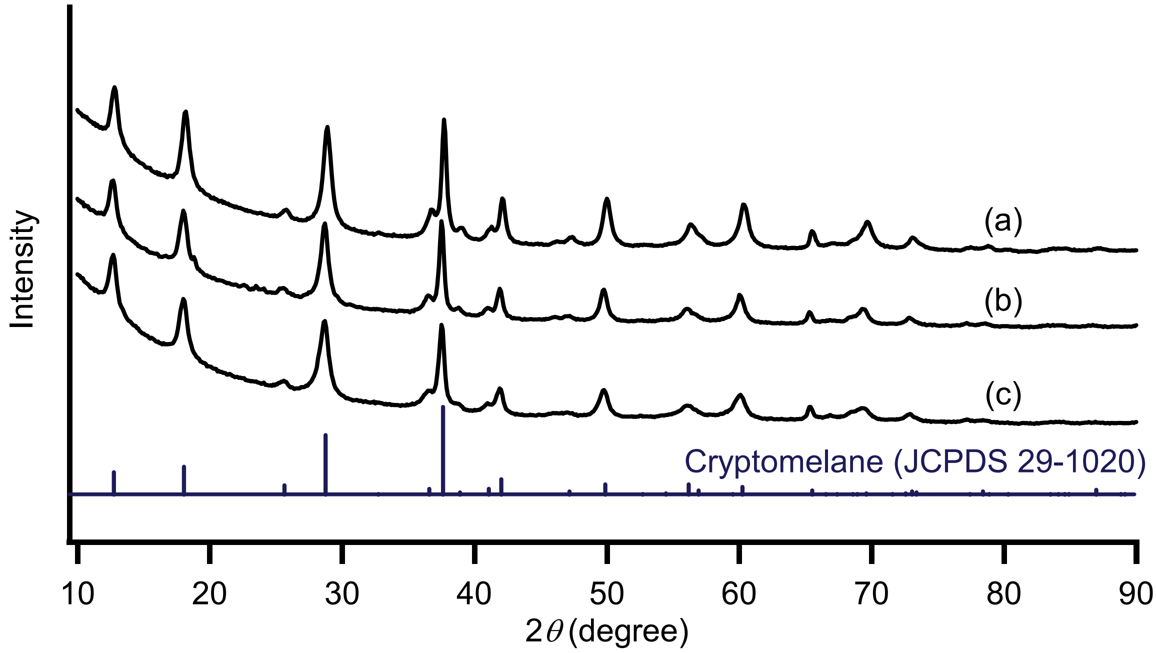

Fig. 2 XRD patterns of (a) as-prepared α-MnO_2, (b) α-MnO_2 retrieved after the oxygenation of **1a** under aerobic conditions, and (c) α-MnO_2 retrieved after the oxygenation of **1a** under anaerobic conditions.

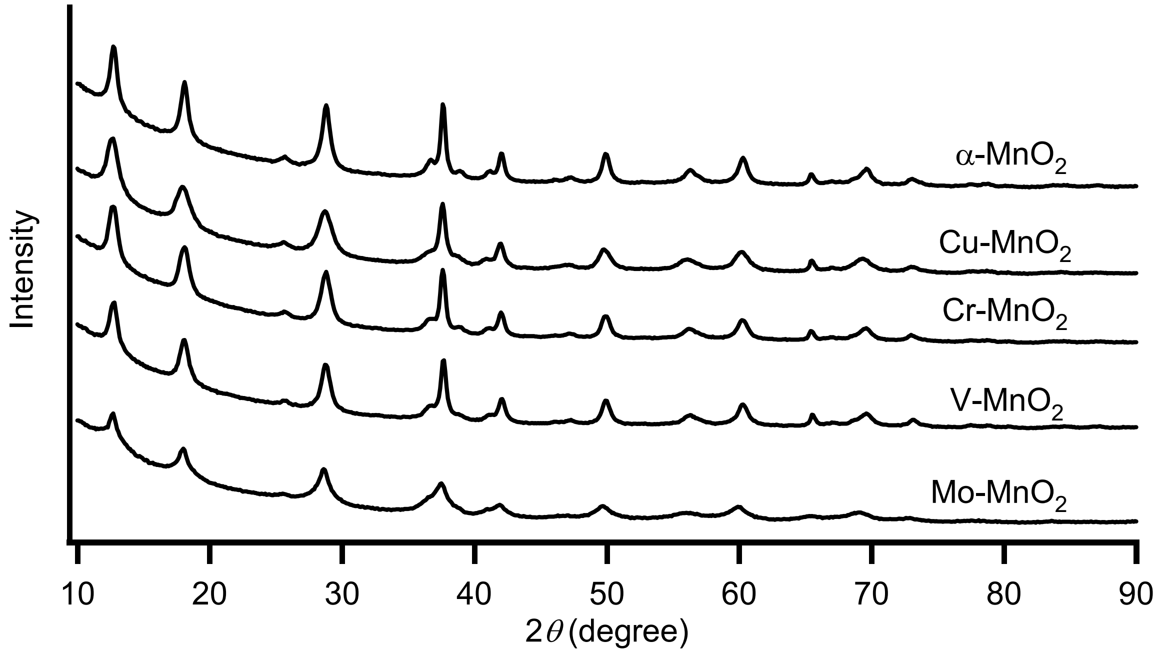

Fig. 3 XRD patterns of α-MnO_2 and M-MnO_2.

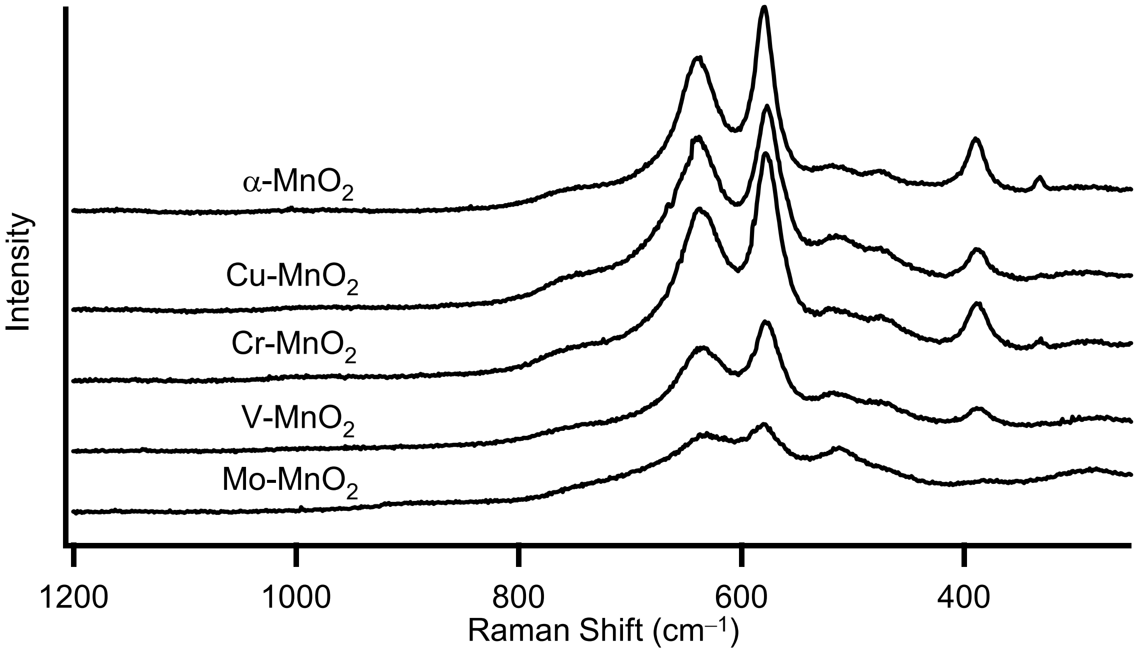

Fig. 4 Raman spectra of α-MnO_2 and M-MnO_2.

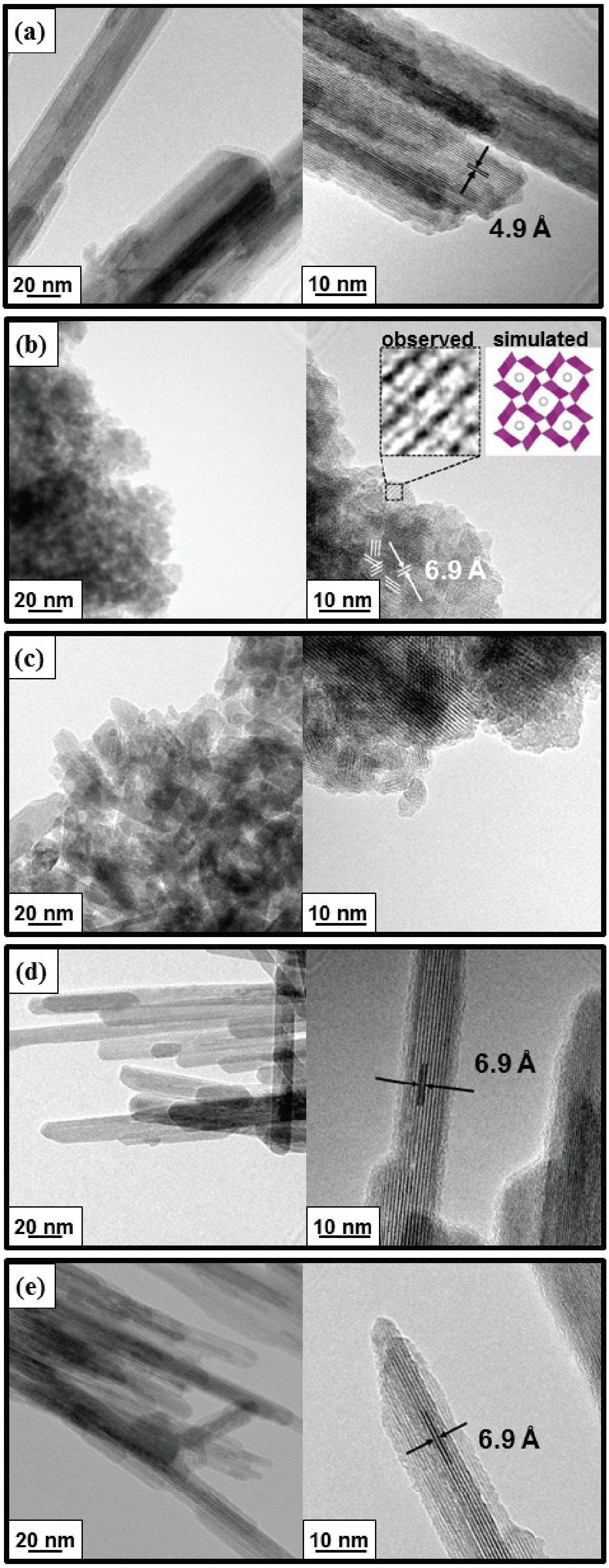

Fig. 5 TEM images of (a) α-MnO_2, (b) Mo-MnO_2, (c) V-MnO_2, (d) Cr-MnO_2, and (e) Cu-MnO_2.

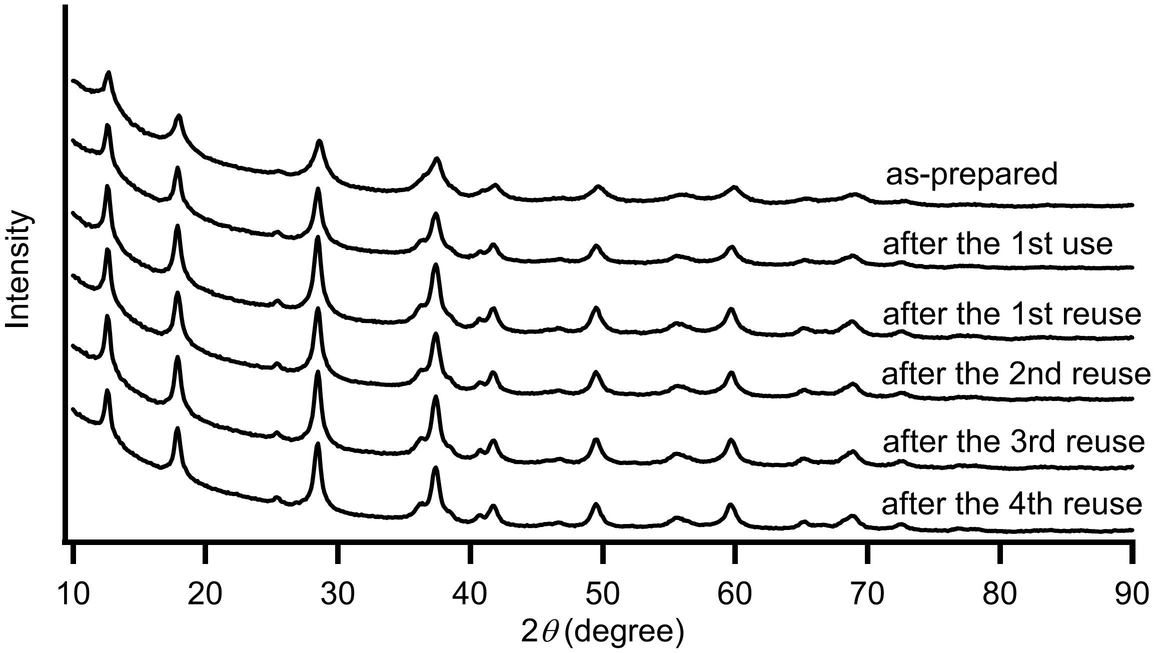

Fig. 6 XRD patterns of as-prepared Mo-MnO_2 and the retrieved Mo-MnO_2 after the use for the oxygenation of **1a** under the conditions described in Table 6 for 6 h.

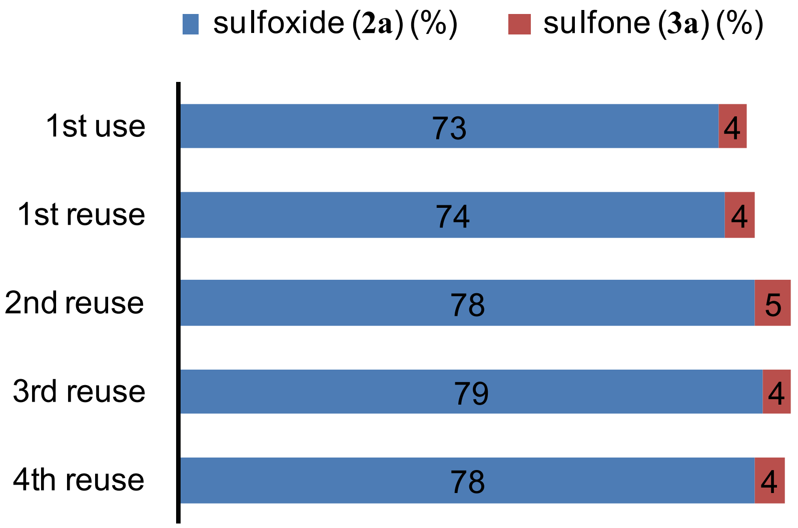

Fig. 7 Reuse experiments of Mo-MnO_2 for the oxidation of **1a**. The reactions were carried out under the conditions described in Table 6 for 6 h. Yields were determined by GC analysis using naphthalene as an internal standard. The retrieved catalyst was washed with acetone and water, and then dried at room temperature prior to being used for the next reuse experiment.

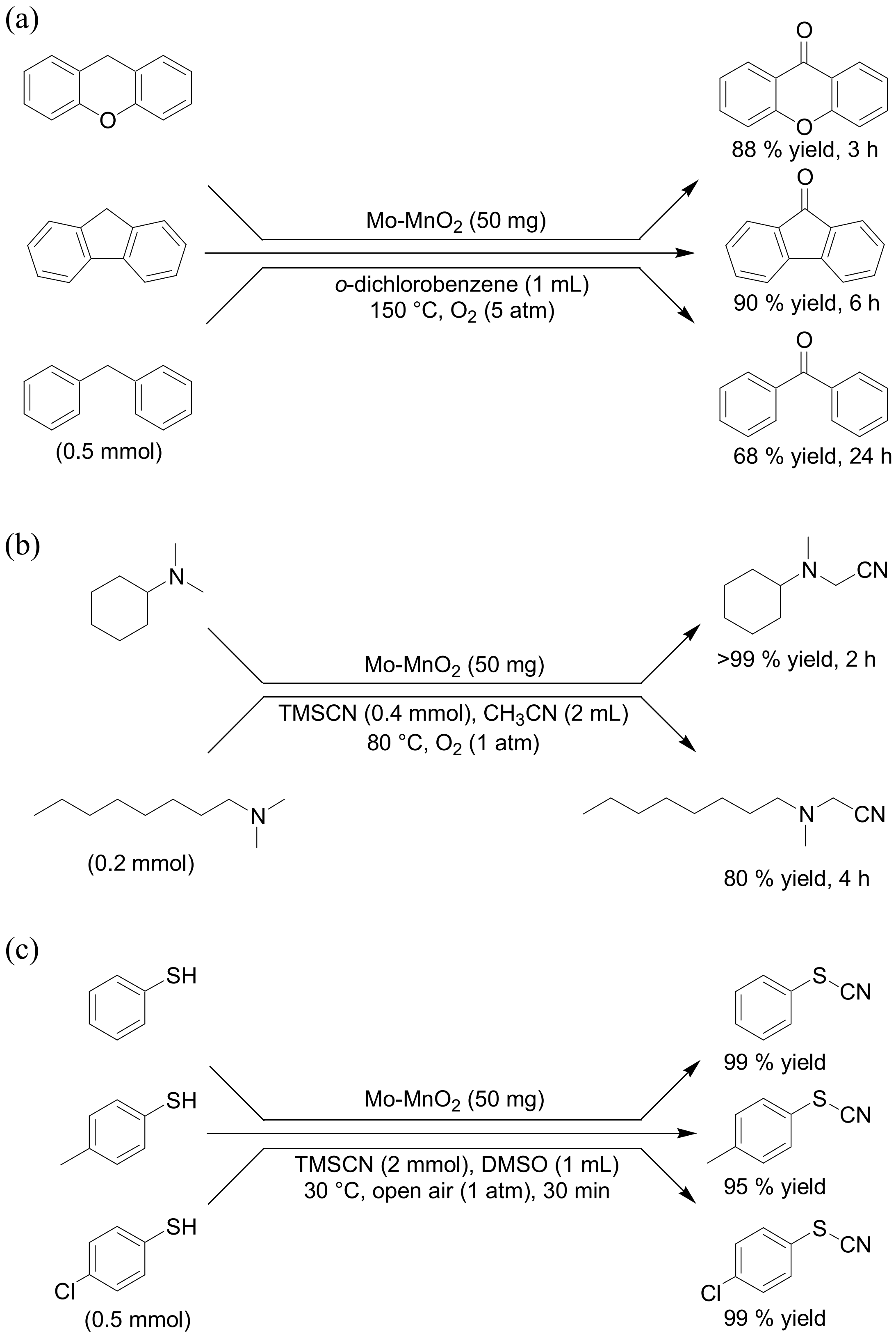

Fig. 8 Several oxidative functional group transformations using Mo-MnO_2: (a) Oxygenation of alkylarenes, (b) oxidative α-cyanation of trialkylamines, and (c) oxidative S-cyanation of benzenethiols.

Graphical abstract

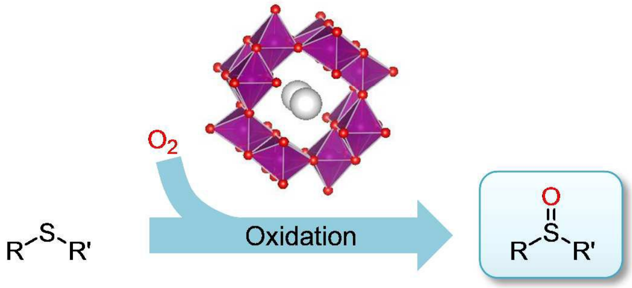

In the presence of Mo^{6+}-doped α-MnO_2 (Mo-MnO_2), various sulfides could efficiently be oxidized to the corresponding sulfoxides as the major products. In addition, Mo-MnO_2 could repeatedly be reused.